第 48 卷 第 6 期/2021 年 3 月/中国激光 研究论文

中国激光

Q960E 钢激光熔覆 Ni 基 WC 涂层组织及性能

胡登文，刘艳*，陈辉**，王梦超

西南交通大学材料科学与工程学院，四川 成都 610031

摘要 为了增强 Q960E 钢的抗磨粒磨损性能，设计出了一种低裂纹敏感性的镍基碳化钨(WC)合金粉末。以气雾化法制备的 WC 和 NiCuBSi 球形粉末按照质量比 3∶7 混粉，通过预热和保温处理，在 Q960E 钢表面制备了无明显裂纹的 Ni 基 WC 耐磨涂层。通过扫描电子显微镜(SEM)、X 射线能量色散谱方法(EDS)、X 射线衍射(XRD)、光学显微镜、维氏硬度计对熔覆层显微组织、元素分布、物相、磨损形貌、截面硬度进行分析，并对熔覆层和 960E 钢的耐磨性能进行了对比测试。涂层中 WC 和 W_2C 是主要的强化相，大颗粒的球形 WC 硬度大于 1500 HV，提高熔覆层的耐磨性；而 Ni 和 Cu 是主要的黏结相，增强涂层的韧性。由于大颗粒的 WC 球有效阻碍了磨粒的压入和犁削，Ni-WC 熔覆层的抗磨粒磨损性能达 Q960E 基材的 6 倍以上，能够有效提高 Q960E 钢的抗磨粒磨损性能。

关键词 激光技术；激光熔覆；Q960E；Ni 基 WC 涂层；磨粒磨损

中图分类号 TG47；TG178 **文献标志码** A **doi**：10.3788/CJL202148.0602120

1 引 言

Q960E 钢是一种低合金高强钢，因可焊接性较好，广泛应用于工程机械、压力容器、地铁车辆等领域[1-3]。经过调质处理后，Q960E 钢的屈服强度大于等于 960 MPa，抗拉强度大于等于 1000 MPa，−40 ℃下纵向冲击功(AKV)大于等于 34 J，是板材中强度级别和冲击韧性较高的钢种。工程机械使用的 Q960E 钢板经常与沙土、砾石等直接接触，产生大量的磨损，造成机械零部件失效，增加了使用成本。激光熔覆通过激光将粉末熔化并使其沉积到基体表面，具有稀释率低、热影响区小、结合强度高等优点，广泛用于涂层制备和修复再制造领域。通过激光熔覆，在较低硬度材料表面熔覆耐磨层，可以保证基体性能的同时有效提高其耐磨、耐腐蚀等性能[4-8]。

尹燕等[9]在 3Cr13 不锈钢表面激光熔覆制备高铬铁基合金，其硬度达基体的 1.9 倍左右。员霄等[10]在 H13 钢表面熔覆 Fe 基和 Co 基熔覆层，耐磨性能明显提高。易伟等[11]通过激光熔覆原位合成了含 NbC 的 Co 基涂层，当 NbC 含量达 10%时，涂层的显微硬度和耐磨性达到最佳。Zou 等[12]在 Invar 合金上激光原位合成了纳米结构的 Cr_3C_2-VC/Co 熔覆层，提高了耐磨性和抗氧化性。李美艳等[13]在 45 钢表面熔覆 Ni-WC/Cr_3C_2 涂层，耐磨性和耐腐蚀性显著提高。徐国建等[14]在低碳钢表面熔覆 Stellite-6 和 VC 混合粉末，根据不同的 VC 比例，熔覆层组织呈现出亚共晶组织和过共晶组织两种类型。亚共晶组织由富钴的 γ 相与共晶组织组成，过共晶组织由初晶 VC 相与共晶组织组成。曹俊等[15]通过在 AISI H13 钢表面制备了不同 WC 含量的 Fe 基涂层，发现添加 WC 后细化了晶粒，并发生了弥散强化，熔覆层的组织和性能得到改善。于浩等[16]研究了不同回火温度下 Q960 钢的组织和分布，给出了回火温度对析出物组织特征的影响规律，随着回火温度的升高，Nb、V 和 Ti 的复合碳氮化物长大，形状也由方形向椭圆形演变。李丹晖等[17]开发了 Q960 高强钢气体来保护焊丝，焊丝焊态熔覆金属抗拉强度为 920 MPa，−60 ℃温度下冲击吸收能量为 66.7 J。

目前为止，尚未发现有关 Q960E 钢表面激光熔

收稿日期：2020-09-04；**修回日期**：2020-10-06；**录用日期**：2020-11-12

基金项目：国家重点研发计划(2017YFB0305900)

* **E-mail**：liuyanzt@163.com；** **E-mail**：xnrpt@swjtu.edu.cn

覆改性研究的成果。Q960E 钢作为工程机械用钢，在长期使用过程中应避免裂纹产生，防止裂纹扩展。激光熔覆的关键是不产生明显裂纹，目前激光熔覆中应用最为广泛的是 Ni60-WC 粉末，由于 Ni60 熔覆层硬度较高，开裂很难避免[18]。因此，需要设计一种兼具高韧性和高耐磨的熔覆涂层。

2 试验方法

试验用基体材料为 Q960E 钢，成分如表 1 所示，线切割 200 mm×50 mm×20 mm 试块。设计了一种低裂纹敏感性的镍基碳化钨合金粉末，成分如表 1 所示。其中，强化相 WC 和 NiCuBSi 黏结相分别通过气雾化法制备，筛选出的粉末粒径为 50～100 μm，按照质量比 m(WC)∶m(NiCuBSi)=3∶7 在混料机中进行混粉，实现 WC 和 NiCuBSi 粉末的均匀分布。镍基碳化钨合金粉末熔覆前在 100 ℃电炉中烘干，烘干时间为 1 h。熔覆前将 Q960E 基体材料放入电炉中预热到 150 ℃，时间为 1 h。将电阻式铸铝加热板放置在熔覆平台上，设置保温温度为 150 ℃，待炉中预热完成后取出样品，放在加热板上，基体的预热温度控制在 150 ℃。熔覆完成后将试样放入炉中温度 150 ℃下保温 4 h，降低残余应力。

表 1 Q960E 和 Ni 基 WC 粉末化学成分的质量分数

Table 1 Mass fraction of chemical composition of Q960E and Ni-based WC powder unit: %

Material	C	Si	Mn	Cu	B	Ni	Cr	Mo	Fe	W
Q960E	0.15	0.5	1.5			1.2	0.8	0.7	Bal.	
Ni-WC	1.2	1.5		14	0.75	Bal.				30

激光熔覆在 IPG YLS-4000 激光器系统上开展，该系统配备了功率为 4.0 kW 的光纤激光器和焦距为 300 mm 的同轴激光熔覆头，用高纯氩气作为保护气和送粉气体。经过优化后，选择的激光熔覆工艺参数如表 2 所示。

表 2 Ni-WC 激光熔覆工艺参数

Table 2 Process parameters of Ni-WC laser cladding

Laser power / W	Powder feeding / (g·min^{-1})	Scanning velocity / (mm·min^{-1})	Shielding gas flow / (L·min^{-1})	Carrier gas flow / (L·min^{-1})	Overlap rate / %
1800	14	250	30	5	50

将激光熔覆后的样品用线切割切成 8 mm×8 mm 的小块，沿着截面方向制备金相试样。用 Cu 靶 X 射线衍射仪对涂层进行物相分析，加速电压为 40 kV，扫描范围为 20°～90°。用蔡司体式光学显微镜(Stemi 2000-C)和场发射扫描电子显微镜(FE-SEM；JSM-7800F，JEOL)对熔覆层显微组织和元素分布进行分析；在显微维氏硬度计(MICRO-586)上使用 1.96 N 的载荷和 15 s 的停留时间测试显微硬度。基于 ASTM G65-2016 标准的仪器，磨粒磨损测试设备将橡胶轮改为相同尺寸的碳化硅 GC60K$_5$ 砂轮，以测试磨损性能，样品的载荷为 130 N，砂轮的直径为 229 mm，磨损转数为 200。磨损后的形貌用光学显微镜进行观察。

3 分析与讨论

3.1 显微组织及元素分析

3.1.1 母材及熔覆层显微组织

图 1 为 Q960E 基材和 Ni-WC 熔覆层的宏观形貌和显微组织图。图 1(a)是熔覆层表面形貌图，熔覆层表面成形较好，其表面 5 个点是测试显微硬度的痕迹。图 1(b)是截面的光学显微照片，可以看出，熔覆层与基材形成了良好的冶金结合，涂层中无明显的气孔和裂纹。对熔覆后的样品切样进行剪切强度测试，4 个样品测试的结果分别为 411.25 MPa、366.46 MPa、382.56 MPa 和 427.18 MPa，表明熔覆层与母材呈现良好的冶金结合。图 1(c)是熔覆样品剪切破坏后的宏观金相图，断口位置位于熔覆层和母材的界面。图 1(d)为剪切样品断口形貌图，可以看出明显的颗粒痕迹，说明 WC 球的存在降低了熔覆层和母材的结合强度，导致界面处断裂。图 1(e)是 Ni-WC 熔覆层金相组织图，有较多的球状颗粒弥散分布在涂层中。图 1(f)是熔覆界面及基材金相组织图，由于激光热输入，在基材靠近熔覆层有 1 mm 左右的热影响区，但是由于 Q960E 钢经过高温回火处理，热输入对热影响区组织影响不大。图 1(g)中熔覆层主要由圆球状的 WC 颗粒和 Ni、Cu 柱状晶组织构成，无明显的裂纹出现。球状 WC 颗粒尺寸为 50～100 μm，分布在涂层中，另外还有小部分 WC 球分解的白色小颗粒 W_2C 均匀弥散分布在涂层中。图1(h)是Q960E基材的扫描电子显微

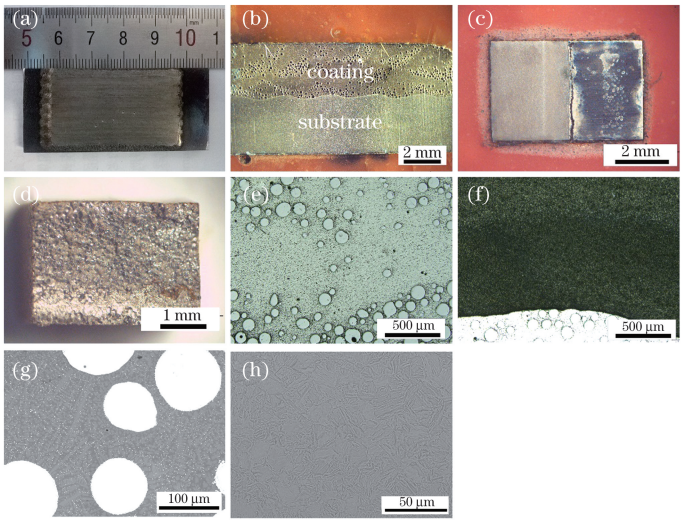

图 1 Ni-WC 熔覆宏观形貌和显微组织图。(a)激光熔覆宏观照片;(b)熔覆界面显微照片;(c)熔覆样品剪切破坏后照片;(d)剪切样品断口形貌图;(e) Ni-WC 熔覆层金相组织图;(f)熔覆界面及基材金相组织图;(g) Ni-WC 熔覆层的 SEM 图;(h) Q960E 基材的 SEM 图

Fig. 1 Macro morphology and microstructure of the Ni-WC cladding. (a) Macro photographs of laser cladding; (b) micrographs of the cladding interface; (c) photograph of cladding sample after shear failure; (d) fracture topography of sheared sample; (e) metallographic structure of Ni-WC cladding layer; (f) metallographic structure of cladding interface and substrate; (g) SEM diagram of Ni-WC cladding layer; (h) SEM diagram of Q960E substrate

镜(SEM)图,其主要是具有马氏体位向的回火索氏体组织,保证了母材具有较高的强韧性。

3.1.2 熔覆层元素分布

图 2 为熔覆层组织的 SEM 形貌和面扫能谱测试结果。图 2(a)中球形相为 WC 颗粒,边缘存在微溶的组织,周围不规则形状的絮状物为激光熔覆过程中球形 WC 分解的 W_2C 小颗粒,这增加了强化相 WC 与黏结相 Ni、Cu 的结合强度,与 Yang 等[19]的研究结果一致。图 2(b)~(e)为能谱面扫结果,表明球状组织、析出的白色球状和小颗粒组织主要成分为 W 元素和 C 元素,黏结相组织主要由 Ni、Cu 元素构成,具体的元素质量分数是 C 为 8.9%,Cu 为 3.5%,Ni 为 31.2%,W 为 56.4%。

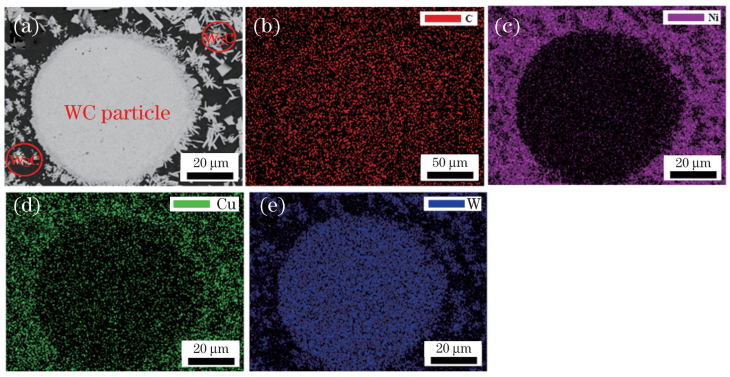

图 2 Ni-WC 熔覆层组织的 SEM 图及 EDS 元素分布图。(a)熔覆层显微组织图;(b) C 元素分布;(c) Ni 元素分布;(d) Cu 元素分布;(e) W 元素分布

Fig. 2 SEM and EDS distributions of microstructure of Ni-WC cladding layer. (a) Microstructure diagram of the cladding layer; (b) distribution of element C; (c) distribution of element Ni; (d) distribution of element Cu; (e) distribution of element W

3.1.3 熔覆层物相测试

图 3 为熔覆层组织的 X 射线衍射(XRD)图。根据 XRD 显示,由于 Ni、Cu 的峰强度很高且接近,难以明显区分。涂层主要的物相是 Ni、Cu、WC、

W_2C、Ni_3B。在熔覆过程中，在激光作用下，部分球形 WC 颗粒分解，生成了 W_2C 絮状小颗粒。激光作用过程中，部分 Ni 与 B 发生原位反应生成了 Ni_3B，增强了涂层的强度，反应式为

$$WC \rightarrow W_2C + C, \tag{1}$$

$$3Ni + B \rightarrow Ni_3B。 \tag{2}$$

在涂层中，WC 和 W_2C 是主要的强化相，提高熔覆层的耐磨性；而 Ni 和 Cu 的延展性和润湿性能较好，是主要的黏结相，增强涂层的韧性。高耐磨相和高强韧相复合，能够有效实现高强韧涂层的制备。

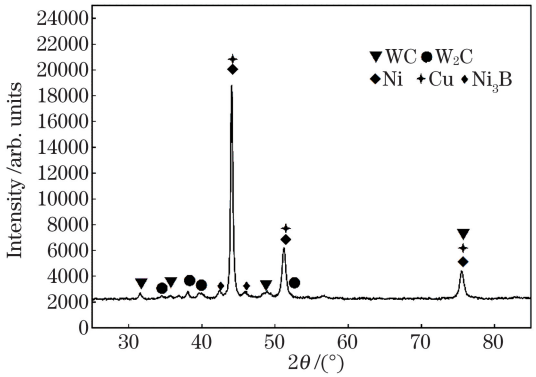

图 3　Ni-WC 熔覆层的 XRD 图

Fig. 3　XRD pattern of Ni-WC cladding layer

3.2　显微硬度分析

图 4 为含熔覆层截面的显微硬度测试结果，间隔 0.1 mm 测试一个数据。根据硬度测试结果，主要区域分布为熔覆层、热影响区和基材三个区。熔覆层中，由于 WC 球状颗粒存在，涂层的硬度差异较大。其中硬度压头全部压入 WC 颗粒时，硬度达 1500 HV 以上，涂层中无 WC 颗粒存在的地方，平均硬度为 404 HV。由于 Q960E 经过了调质处理，激光热输入对热影响区和基材硬度影响不明显，热影响区和基材硬度区域的平均硬度为 374 HV 左右。

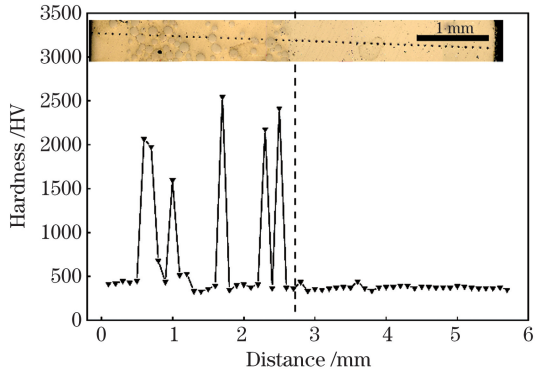

图 4　Ni-WC 熔覆层样品截面显微硬度分布

Fig. 4　Microhardness distribution of sample cross-section of Ni-WC cladding layer

3.3　磨损性能测试

对熔覆前后的样品进行磨粒磨损性能测试，磨损后的形貌如图 5 所示。图 5(a)为 Q960E 钢的磨损形貌图，图中有明显的犁沟和切削划痕。图 5(b)为熔覆层的磨损形貌图，与图 5(a)相比，大颗粒的 WC 球有效阻碍了磨粒的压入和犁削，从而整体的磨损沟槽深度较浅。在相同磨粒磨损实验条件下，对 Q960E 钢和 Ni-WC 熔覆涂层样品进行磨损质量和体积对比，Q960E 钢和 Ni-WC 熔覆涂层样品质量损失分别为 7.568 g 和 1.243 g，用磨损前后损失的质量除以密度，获得磨损体积分别为 0.967 cm^3 和 0.138 cm^3。因此，Ni-WC 熔覆涂层能够有效阻碍硬质砂砾对基体的磨损，增强基体的耐磨性，达 Q960E 基材的 6 倍以上。

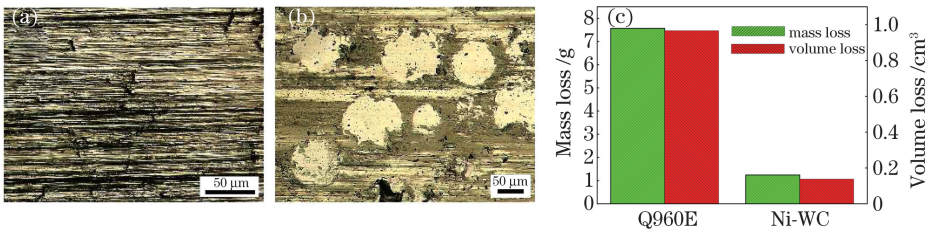

图 5　基材及熔覆层磨损显微形貌及性能对。(a)Q960E 基材磨损形貌图；(b)Ni-WC 熔覆层磨损形貌图；(c)抗磨损性能对比

Fig. 5　Wear micrograph and performance of substrate and cladding layer. (a) Wear topography of Q960E substrate; (b) wear topography of Ni-WC cladding; (c) comparison of wear resistance performance

4　结　　论

设计了一种低裂纹敏感性的镍基碳化钨合金粉末，以气雾化法制备的 WC 和 NiCuBSi 球形粉末按照质量比 3∶7 混粉，通过预热和保温处理，在 Q960E 钢表面制备了无明显裂纹的 Ni 基 WC 耐磨涂层。熔覆层中主要的物相为 WC、W_2C、Ni、Cu 和 Ni_3B。WC 和 W_2C 是主要的强化相，球形 WC 硬度

大于 1500 HV，提高熔覆层的耐磨性；而 Ni 和 Cu 是主要的黏结相，增强涂层的韧性。熔覆后 Ni-WC 涂层的耐磨粒磨损性能达 Q960E 基材的 6 倍以上，主要是因为大颗粒的 WC 球有效阻碍了磨粒的压入和犁削，从而整体的磨损沟槽深度浅，因此，熔覆涂层能够有效阻碍硬质砂砾对基体的磨损。

参 考 文 献

[1] Kan B, Wu W J, Yang Z X, et al. Stress-induced hydrogen redistribution and corresponding fracture behavior of Q960E steel at different hydrogen content [J]. Materials Science and Engineering: A, 2020, 775: 138963.

[2] Wang S Y, Yu H, Zhou T, et al. Synergetic effects of ferrite content and tempering temperature on mechanical properties of a 960 MPa grade HSLA steel [J]. Materials (Basel, Switzerland), 2018, 11(10): E2049.

[3] Bai F M, Zhou H W, Liu X H, et al. Masing behavior and microstructural change of quenched and tempered high-strength steel under low cycle fatigue [J]. Acta Metallurgica Sinica (English Letters), 2019, 32(11): 1346-1354.

[4] Luo X, Li J, Li G J. Effect of NiCrBSi content on microstructural evolution, cracking susceptibility and wear behaviors of laser cladding WC/Ni-NiCrBSi composite coatings [J]. Journal of Alloys and Compounds, 2015, 626: 102-111.

[5] Li Y N, Li Z G, Wang X X, et al. Fe-based wear-resistant coating on railroad switch prepared using laser cladding technology and its properties [J]. Chinese Journal of Lasers, 2020, 47(4): 0402009.
李英男, 李铸国, 王晓翔, 等. 道岔尖轨表面的激光熔覆铁基耐磨涂层及其性能[J]. 中国激光, 2020, 47(4): 0402009.

[6] Mazaheri Tehrani H, Shoja-Razavi R, Erfanmanesh M, et al. Evaluation of the mechanical properties of WC-Ni composite coating on an AISI 321 steel substrate[J]. Optics & Laser Technology, 2020, 127: 106138.

[7] Li M Y, Han B, Song L X, et al. Enhanced surface layers by laser cladding and ion sulfurization processing towards improved wear-resistance and self-lubrication performances [J]. Applied Surface Science, 2020, 503: 144226.

[8] Chen J F, Li X P, Xue Y P. Friction and wear properties of laser cladding Fe901 alloy coating on 45 steel surface[J]. Chinese Journal of Lasers, 2019, 46(5): 0502001.
陈菊芳, 李小平, 薛亚平. 45 钢表面激光熔覆 Fe901 合金的摩擦磨损性能[J]. 中国激光, 2019, 46(5): 0502001.

[9] Yin Y, Pan C L, Zhao C, et al. Formation mechanism of microstructure of laser cladding high chromium Fe-based alloy and its effect on microhardness[J]. Transactions of the China Welding Institution, 2019, 40(7): 114-120, 166.
尹燕, 潘存良, 赵超, 等. 激光熔覆高铬铁基合金的组织形成机制及对显微硬度的影响[J]. 焊接学报, 2019, 40(7): 114-120, 166.

[10] Yuan X, Wang J, Zhu Q H, et al. Microstructure and abrasion resistance of Fe-based and Co-based coatings of AISI H13[J]. Transactions of the China Welding Institution, 2018, 39(12): 105-109, 133.
员霄, 王井, 朱青海, 等. H13 钢的铁基和钴基熔覆层组织与耐磨性[J]. 焊接学报, 2018, 39(12): 105-109, 133.

[11] Yi W, Chen H, Wu Y, et al. Effect of *in situ* NbC on microstructure and wear properties of laser cladding Co-based coatings [J]. Chinese Journal of Lasers, 2020, 47(3): 0302010.
易伟, 陈辉, 吴影, 等. 原位 NbC 对激光熔覆 Co 基涂层组织和磨损性能的影响[J]. 中国激光, 2020, 47(3): 0302010.

[12] Zou Y, Ma B H, Cui H C, et al. Microstructure, wear, and oxidation resistance of nanostructured carbide-strengthened cobalt-based composite coatings on Invar alloys by laser cladding [J]. Surface and Coatings Technology, 2020, 381: 125188.

[13] Li M Y, Han B, Wang Y, et al. Study on microstructure and property of laser cladded Ni-WC/Cr_3C_2 coating[J]. Transactions of the China Welding Institution, 2016, 37(3): 17-21, 129-130.
李美艳, 韩彬, 王勇, 等. 激光熔覆 Ni-WC/Cr_3C_2 涂层组织及性能[J]. 焊接学报, 2016, 37(3): 17-21, 129-130.

[14] Xu G J, Li C G, Guo Y Q, et al. Organization of clad layer using mixed powder of Stellite 6 and VC [J]. Transactions of the China Welding Institution, 2017, 38(6): 73-78, 132.
徐国建, 李春光, 郭云强, 等. 激光熔覆 Stellite-6+VC 混合粉末的熔覆层组织[J]. 焊接学报, 2017, 38(6): 73-78, 132.

[15] Cao J, Lu H F, Lu J Z, et al. Effects of tungsten carbide particles on microstructure and wear resistance of hot-working die prepared via laser cladding[J]. Chinese Journal of Lasers, 2019, 46(7): 0702001.
曹俊, 卢海飞, 鲁金忠, 等. WC 对激光熔覆热作模具的组织和磨损性能的影响[J]. 中国激光, 2019, 46(7): 0702001.

[16] Yu H, Zhang D D, Xiao R T, et al. Effect of tempering temperature on the structural properties of precipitates in Q960 steel[J]. Journal of University of Science and Technology Beijing, 2011, 33(6): 715-720.
于浩, 张道达, 肖荣亭, 等. 回火温度对 Q960 钢析出物组织特征的影响[J]. 北京科技大学学报, 2011, 33(6): 715-720.

[17] Li D H, Xu Y N, Xu H, et al. Analysis on microstructure and mechanical properties of 960 MPa deposited metal[J]. Welding & Joining, 2017(2): 44-47, 71.
李丹晖, 徐亦楠, 徐浩, 等. Q960 高强钢焊丝熔敷金属组织及性能研究[J]. 焊接, 2017(2): 44-47, 71.

[18] Zhang P X, Pang Y B, Yu M W. Effects of WC particle types on the microstructures and properties of WC-reinforced Ni60 composite coatings produced by laser cladding[J]. Metals, 2019, 9(5): 583.

[19] Yang J X, Xiao Z Y, Yang F, et al. Microstructure and magnetic properties of NiCrMoAl/WC coatings by laser cladding: effect of WC metallurgical behaviors[J]. Surface and Coatings Technology, 2018, 350:110-118.

Microstructure and Properties of Laser Cladding Ni-based WC Coating on Q960E Steel

Hu Dengwen, Liu Yan*, Chen Hui**, Wang Mengchao

School of Material Science and Engineering, Southwest Jiaotong University, Chengdu, Sichuan 610031, *China*

Abstract

Objective Q960E steel is a low alloy high-strength steel. It is widely used in construction machinery, pressure vessels, and subway vehicles due to its good weldability. The Q960E steel plate used in construction machinery often comes into direct contact with sand and gravel, causing wear and tear which can lead to failures of mechanical parts and increase usage costs. The key to laser cladding of Q960E steel is to produce no obvious cracks. At present, the most widely used laser cladding wear-resistant powder is Ni60-WC, due to the high hardness of the Ni60 cladding layer, it is difficult to avoid cracking. Therefore, in this study, we designed a Ni-based WC composite powder with both high toughness and high wear resistance. The powder is deposited on the Q960E substrate by laser cladding; through preheating and heat preservation treatment, a wear-resistant coating without obvious cracks can be prepared, and the wear resistance is improved.

Methods The test substrate material is Q960E steel, which was wire-cut into a test block of 200 mm × 50 mm × 20 mm. The low crack sensitivity nickel-based tungsten carbide alloy powder was designed, and the WC reinforced phase and NiCuBSi bonded phase was prepared by aerosolization. The two were mixed at a mass ratio of 3∶7 (Table 1). The nickel-based tungsten carbide powder was dried in an electric furnace at 100 ℃ for 1 h. Before the cladding, the Q960E substrate was put into the electric furnace at 150 ℃ for 1 h. The resistive cast aluminum heating plate was placed on the cladding platform, and the holding temperature was set at 150 ℃. After the preheating in the furnace was complete, the sample was taken out and placed on the heating plate to keep the preheating temperature of the matrix under control at 150 ℃. After the completion of cladding, the sample was put into the furnace at 150 ℃ for 4 h to reduce the residual stress. The microstructure, element distribution, phase, wear morphology, and cross-sectional hardness of the cladding layer were analyzed by scanning electron microscope (SEM), EDS, X-ray diffraction(XRD), optical microscope, and Vickers hardness tester. The wear resistance of the cladding layer and that of the 960E steel were tested and compared.

Results and Discussions A good metallurgical bonding was formed between the cladding layer and the substrate. No obvious pores or cracks appeared in the coating, and it was well-formed with spherical WC particles diffusely distributed in the coating (Fig. 1). The tested shear strengths of the cladding and substrate are 411.25 MPa, 366.46 MPa, 382.56 MPa, and 427.18 MPa. The location of the fracture is at the interface between the cladding and the base material, indicating that the presence of WC spherical particles will reduce the bonding strength between the cladding and the substrate, resulting in fracture at the interface. The spherical phase is WC particles with a slightly soluble structure at the edge. The surrounding irregular shape flocs for the laser cladding process of spherical WC decomposition of W_2C particles, increasing the bonding strength of the reinforced phase WC and the bonding phase

Ni, Cu (Fig. 2). The main phases of the coating are composed of Ni, Cu, WC, W_2C, and Ni_3B (Fig. 3). In the process of cladding, under the action of the laser, part of the spherical WC particles decomposed and W_2C floc-like small particles were generated. Part of Ni reacted with B *in-situ* to generate Ni_3B, which enhanced the strength of the coating. In the cladding layer, the hardness of the coating varied greatly due to the existence of WC spherical particles. When the hardness head was all pressed into WC particles, the hardness reaches more than 1500 HV; where no WC particles existed in the coating, the average hardness is 404 HV. Because the Q960E had been tempered, the effect of laser heat input on the hardness of the heat-affected area and the base material was not obvious; the average hardness of heat-affected area and base material hardness area is about 374 HV (Fig. 4). The wear morphology of the Q960E steel showed obvious plowing grooves and cutting scratches; the wear morphology of the cladding layer showed that the large particles of WC balls effectively prevented the abrasive particles from pressing in and plowing, resulting in an overall shallow wear groove depth (Fig. 5). Comparison of the wear mass and volume showed that the mass losses of the Q960E steel and the Ni-WC melt-coated samples are 7.568 g and 1.243 g, respectively. The wear volume was obtained by dividing the mass loss before and after wear by the density, to obtain 0.967 cm^3 and 0.138 cm^3, respectively.

Conclusions A Ni-based tungsten carbide alloy powder with low crack susceptibility was designed, and WC and NiCuBSi spherical powders prepared by aerosolization were mixed according to the mass ratio of 3∶7. The Ni-based WC wear-resistant coating without obvious cracks was prepared on the surface of Q960E steel by a preheating and holding treatment. The main phases in the cladding layer are WC, W_2C, Ni, Cu, and Ni_3B. WC and W_2C are the main reinforcing phases, and the hardness of spherical WC is more than 1500 HV, which improves the wear resistance of the cladding layer. Ni and Cu are the main bonding phases, which enhance the toughness of the coating. The wear resistance of the Ni-WC coating after cladding is more than 6 times that of the Q960E substrate, mainly due to the large particles of WC spheres effectively hindering the abrasive particles from pressing in and plowing. The overall depth of the wear groove was not deep; therefore, the cladding coating can effectively hinder the wear of hard gravel on the substrate.

Key words laser technique; laser cladding; Q960E; Ni-based WC coating; abrasive wear

OCIS codes 140.3390; 160.3900